International Journal of Remote Sensing

ISSN: 0143-1161 (Print) 1366-5901 (Online) Journal homepage: www.tandfonline.com/journals/tres20

Prediction and mapping of boreal forest fire fuel loads using high-resolution satellite stereo imagery

Ranjith Gopalakrishnan, Lauri Korhonen, Matti Maltamo, Syed Adnan & Petteri Packalen

To cite this article: Ranjith Gopalakrishnan, Lauri Korhonen, Matti Maltamo, Syed Adnan & Petteri Packalen (2025) Prediction and mapping of boreal forest fire fuel loads using high-resolution satellite stereo imagery, International Journal of Remote Sensing, 46:21, 8028-8050, DOI: 10.1080/01431161.2025.2562006

To link to this article: https://doi.org/10.1080/01431161.2025.2562006

Published online: 06 Oct 2025.

INTERNATIONAL JOURNAL OF REMOTE SENSING
2025, VOL. 46, NO. 21, 8028–8050
https://doi.org/10.1080/01431161.2025.2562006

Taylor & Francis
Taylor & Francis Group

Prediction and mapping of boreal forest fire fuel loads using high-resolution satellite stereo imagery

Ranjith Gopalakrishnan[a], Lauri Korhonen[a], Matti Maltamo[a], Syed Adnan[b] and Petteri Packalen[c]

[a]School of Forest Sciences, Faculty of Science and Forestry, University of Eastern Finland, Joensuu, Finland; [b]Oy Arbonaut Ltd., Joensuu, Finland; [c]Natural Resources Institute Finland (Luke), Bioeconomy and Environment Unit, Helsinki, Finland

ABSTRACT

The aim of this study is to evaluate the suitability of very high-resolution satellite stereo-imagery data for creating forest fire-related fuel load maps in the boreal region. We acquired stereo imagery from the GeoEye-1 (GE-1) satellite, which has a ground sampling distance of 50 cm. The images were acquired in August 2021 and 2023 (hence leaf-on). Our study area was centred around the Hiidenportti national park in central Finland, dominated by natural boreal forests. The ground reference was a field dataset consisting of measurements from 33 forested plots, each of 15 m radius. The dominant height (m), foliage biomass (t ha-1) and canopy base height (m) were predicted using multivariate linear regression models, while the understory presence (categorical; present/absent) was predicted using logistic regression analysis. Prediction models using area-based metrics based on airborne laser scanning (ALS) data had the smallest associated root mean square error (RMSE) (between 2.6% and 23.9%). Meanwhile, similar type of area-based metrics of stereo satellite data combined with an ALS-based digital terrain model (DTM) resulted in RMSEs of 6.6–30.3%. We also formulated models suitable for the case when only satellite data is available (i.e. high-quality DTM is absent), such as in remote locations of the boreal forest region. In this case, the models involved several canopy texture metrics and point cloud height and colour intensity-based metrics as predictors. The associated relative RMSEs were in the range of 11–30%. Dominant height, an important global vegetation metric, was predicted with an RMSE of 2.6 m, which compares well with other model predictions under similar circumstances. Our findings suggests that very high-resolution stereo satellite image data is promising for the generation and updating of wall-to-wall boreal forest fuel load maps, including remote areas lacking high resolution DTM data.

ARTICLE HISTORY
Received 6 June 2025
Accepted 10 September 2025

KEYWORDS
Stereo satellite; high resolution satellite imagery; GeoEye-1; Airborne Laser Scanning; forest fire; DTM-independent

CONTACT Ranjith Gopalakrishnan ranjith.gopalakrishnan@uef.fi School of Forest Sciences, Faculty of Science and Forestry, University of Eastern Finland, Borealis building, Yliopistokatu 7, Joensuu 80130, Finland

1. Introduction

Changes in global wildfire regimes caused by several factors including climate change is a cause of concern, with wide-ranging implications for both human and ecosystem health and well-being (Duane, Castellnou, and Brotons 2021). The series of mega-fires that have been seen in the last decade are unprecedented in the worldwide instrumental records and threaten the stability of major global carbon sinks such as that in the Amazon region (Clarke et al. 2022). There are also serious consequences projected for the timber industry: a recent study found wildfire-related global timber-producing forest area losses are substantial and increasing (Bousfield, Lindenmayer, and Edwards 2023). There are around 1000 small (average size < 1 ha) forest fires annually in Finland (Lehtonen et al. 2016). The major reasons for these relatively small fire sizes in the country is the presence of a well-developed fire suppression infrastructure and a dense forest road network. However, there was increased forest fire activity in the region of Sweden and Finland in the years of 2014 and 2018, with respect to long-term climatological averages (Maltamo et al. 2020). Moreover, an increase in the frequency of hot and dry periods is projected for the country in the future, because of a warming climate (Lehtonen et al. 2016). This would lead to augmented forest fire risks in the region.

Remote sensing has played a significant role in guiding forest fire management, such as those related to fuel estimation and related fire risk mapping (Gale et al. 2021). Over the past few decades, three-dimensional (3D) data acquired remotely has emerged as a crucial information source for predicting the spatial characteristics of forest biophysical properties, including those related to forest fire fuel load. Among 3D remotely sensed (RS) technologies, Airborne Laser Scanning (ALS) has received extensive scrutiny for its application in forestry. Its effectiveness in mapping forest biophysical features (such as canopy height, canopy cover, crown dimensions and understory presence) has been thoroughly recorded, particularly within the framework of stand level management inventories and that of ecological and biodiversity surveys (Fassnacht et al. 2024; Stereńczak et al. 2020; Toivonen et al. 2023). Notably, ALS possesses the capability to acquire highly detailed 3D profiles across extensive areas, offering insights into ground elevation and providing in-depth three-dimensional forest characterization. The primary remote sensing data used for operational forest management inventory in Finland is ALS data (Maltamo and Packalen 2014). It has been used in an area-based approach context in conjunction with plot data to derive wall-to-wall maps of important forest fuel load parameters (e.g. see Maltamo et al. 2020). Another interesting and more generalizable alternative of using ALS data is applying the Beer – Lambert law of light extinction to invert ALS return vertical structure to vertically stratified fuel load metrics distributions (Martin-Ducup et al. 2025). Nevertheless, the associated costs of collecting and updating ALS data have been a barrier to its deployment over large areas, such as on a national scale in larger countries. This is especially true for remote (but fire prone) locations of the boreal region, where the lack of supporting infrastructure (roads, aircraft take-off and landing strips, etc.) can drive up costs.

It can be said that the launch of IKONOS satellite in 1999 was the start of a new age in the satellite based remote sensing. Since then, a number of so-called very high-resolution (VHR) optical earth observation satellites have been launched, with the ground sampling distance (GSD) of associated PAN images being ~1 m or less. Around 25 of them (including constellations) have been launched since 1999; they are listed in a

recent publication (Yin et al. 2023; see Table A.1). The GeoEye-1 satellite, launched in 2008, is one of them and is the source of images used in this article. The GSD of the panchromatic images acquired by the GeoEye-1 satellite is 46 cm at nadir, while the multispectral bands (4 of them) have a coarser resolution of 1.84 m. Moreover, it has the capability to collect in-track stereo images that enables the creation of a 3D model of the vegetation below. The commercial acquisition cost of such stereo imagery is typically ~30 euros per square kilometre. This compares somewhat favourably with that of ALS data; for example, the cost of ALS acquisition in Finland is ~40 euros per km^2 (National land survey of Finland 2023). There have been several previous studies looking at the suitability of using such high-resolution stereo images for forest parameter estimation (Fassnacht et al. 2017; Vastaranta et al. 2018; Wittke et al. 2019). But they may be subject to one or several disadvantages with respect to boreal forests fuel load mapping. Most of them use a set of ground control points (GCPs) to correct the orientation of the images; collection of such GCPs may be infeasible in many remote forested areas. Meanwhile, the importance of the algorithm used for image matching has been demonstrated in the forestry context (Kukkonen, Maltamo, and Packalen 2017). Another important aspect to consider is the software implementation of the algorithm, which can significantly affect vegetation reconstruction from stereo images (Probst, Gatziolis, and Strigul 2018). Most previous studies do not take advantage of improvements in these directions that have happened in the last few years. Lastly, many of them were conducted in the temperate and tropical vegetation zones, and are not representative of the relatively sparse, coniferous dominated boreal forests of the Nordic region.

Many previous similar studies use a high-quality ALS-based DTM as auxiliary data for the processing of the stereo satellite image data (Fassnacht et al. 2017; Liu et al. 2021; Vastaranta et al. 2018). The ground elevation values derived from such a DTM are used to 'normalize' the z-values in the satellite-derived point cloud; i.e. to convert them to height above local ground level. But such a DTM may not be available in many remote (but fire prone) areas, such as the southern edge of the boreal forest region. An alternative is using a global DTM as a substitute. But these may be error prone, especially in forested areas (O'Loughlin et al. 2016; Rizzoli et al. 2017). Meanwhile, a study on the feasibility of predicting forest volume using non-normalized point cloud data from unoccupied aerial vehicles (UAVs) reported encouraging results in both Italian and Norwegian forested regions (Giannetti et al. 2018). The results of that study seem to indicate that one can derive image metrics, which are correlated to various important forest parameters (such as dominant height, timber volume, etc.) even in the absence of a high-quality DTM. In this work, we evaluate the efficacy of similar techniques but in the context of high-resolution stereo satellite data from the GeoEye-1 satellite.

Various fire behaviour models are used by forest managers and stakeholders to assess fire risk and to plan controlled and strategic fuel reduction treatments, such as controlled burning (e.g. FARSITE and *Prometheus*, see Gale et al. 2021). The spatial mapping of various fuel types and quantity is an important input for these models (Chirici et al. 2013). In forested environments, one of the most important fuel parameter input for fire behaviour models is the canopy bulk density (CBD). This is defined as the mass of available canopy fuel (canopy fuel weight) per defined chosen

unit canopy volume (Gajardo, García, and Riaño 2014). It is closely linked to the initiation and propagation of crown fires (Wagner 1977). A simpler version of this parameter estimates only the foliage biomass while the more comprehensive version includes both foliage and tree branches. Another important parameter for fire behaviour models is canopy base height (CBH). This refers to the vertical distance between ground surface and the base of the continuous live crown (i.e. lowest branch of the tree crown with live foliage) (Stefanidou et al. 2020). Given high-quality ALS point cloud data that sufficiently samples all vertical strata of overstory, this can be estimated either from the vertical distribution of the returns or by regression-based methods (Maltamo et al. 2018). Yet another crucial fuel parameter that characterizes the forest understory layer is the surface canopy height (SCH). It is defined as the height of the fuel layer that is situated over the ground fuels but beneath the canopy or aerial fuel (Gajardo, García, and Riaño 2014). A 2-metre threshold has been used by some authors (Labenski et al. 2022); any biomass below it was considered as surface fuel. This usually comprises of grass, shrubs, brush, slash and timber and is important to both fire intensity and spread.

The objective of the present study is to better understand the capabilities of VHR satellite data combined with the latest point cloud generation software techniques to predict forest fuel load related parameters. We focus on the three parameters listed above, given their importance in fire behaviour models. We also try to predict canopy height (quantified as dominant height) as it is an important spatial variable correlated with forest productivity, terrestrial ecosystem functioning, aboveground carbon stock and biodiversity (Skidmore et al. 2021). Surface canopy height is discretized into a binary categorical variable (understory present/absent), in our case. Specifically, we aim to address the following research questions:

1. What is the efficacy of satellite stereo point data for prediction of boreal fuel load parameters, when compared to those from ALS?

2. Can a set of metrics solely derived from satellite data (i.e. no high-quality auxiliary DTM available) be used to predict these fuel load parameters?

By systematically investigating these questions, we help to evaluate the potential of satellite based stereo imagery and orthoimagery as a viable alternative to ALS for both small area and large area mapping of forest parameters.

2. Materials and methods

2.1. Study area

The site for this research study is a 10×10 km area, located around the Hiidenportti National Park, in central Finland (63° 52'N, 29° 4' E). The forest here is part of the middle boreal forest zone, and comprises of a mix of natural and managed forests. The elevation ranges from 160 to 260 m above sea level, with respect to the Finnish N2000 height system. The dominant tree species found here are Scots pine (*Pinus sylvestris* L.) and Norway spruce (*Picea abies* (L.) H. Karst.).

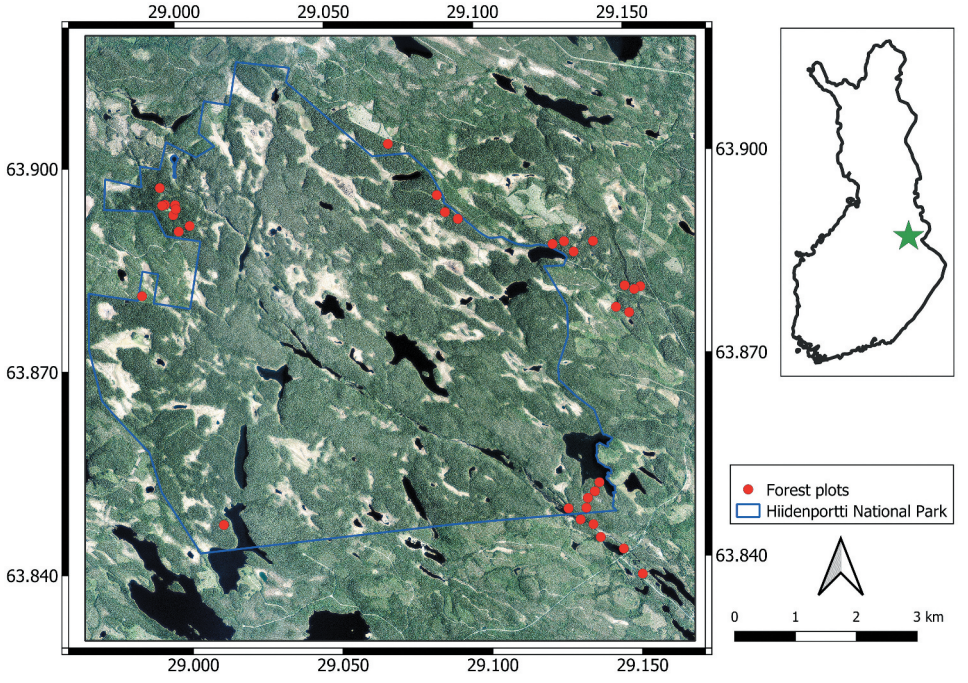

Figure 1. Location of forest plots in the 10 × 10 km study area. The inset map on the right shows the location of the study area in Finland. The background image for the main map is an aerial orthophoto from the year 2020, indicating the major land cover types present.

2.2. Field data

Measurements from 33 fixed radius sample plots were used in this study (Figure 1); all these plots were unaffected by cloud cover in the satellite images (described below). These plots were placed so that they sampled a wide range of forest conditions of the study area with respect to tree species, height and volume. Of these, 29 plots were measured in the summer of 2021, and four additional plots in the summer of 2023. Of the 33 plots, 31 were located in mature or old growth forests that were rich in dead wood. These plots had a radius of 15 m. Meanwhile, two plots were in young stands; these were included to get more height variation in the plot dataset. They had a radius of 10 m. Plot locations were positioned by means of a Trimble Geo 7+ Tornado (with external antenna) global navigation satellite system (GNSS). The GNSS data were corrected afterwards using reference stations (post-correction estimated location accuracy is ±1 m). The diameter at breast height (DBH), tree height and crown base height were measured from all trees having DBH more than 5 cm. The heights were measured using a Haglöf Vertex IV electronic hypsometer. Tree species was also determined for each measured tree. Dominant height was calculated as an average of tree heights of 100 most thickest trees by DBH per hectare. Foliage biomass was predicted using biomass models of Repola (Repola 2008, 2009). The existence of understory in plots was visually assessed during fieldwork. That is, according to visual

Table 1. Statistics associated with the 33 field-measured plots used in this study.

	Mean	Std. dev.	Min.	Max.
Dominant height (m)	23.6	4.0	10.0	30.9
Foliage biomass (leaf on) (t ha^{-1})	7.7	3.8	1.7	18.0
Canopy base height (m)	7.0	2.0	2.1	12.7
Timber volume (m3 ha^{-1})	275.2	98.0	40.4	522.2
Mean diameter (cm)	19.5	4.2	9.6	27.6
Number of stems (ha^{-1})	892.8	353.4	382.0	2387.3
	Present		**Absent**	
Understory presence	22		11	
	Pine	**Spruce**	**Birch and other deciduous**	
Main tree species	11	13	9	

interpretation, plots were classified as either 'understory absent' or 'understory present'. For the plots with understory, the main tree species and mean height of the understory vegetation were visually assessed. Meanwhile, the associated stem number was counted. Salient statistics of plot attributes modelled in this study are shown in Table 1.

2.3. Remote sensing data

2.3.1. Airborne laser scanning (ALS) data

We used ALS data that was collected as part of a periodical national survey by the National Land Survey (NLS) of Finland. As part of this, a Riegl VQ-1560II laser scanner-based system was employed to gather such data across the study area in June 2020 (hence leaf-on conditions). More details about the data acquisition are given in Table 2.

2.3.2. Satellite stereo-imagery

We acquired in-track stereo pairs of satellite images from GeoEye-1, a commercial optical satellite launched in September 2008. The images were acquired over the study area on 28 August 2021 (leaf-on) at approximately 12.30 pm local time. The images were delivered in four rectangular tiles. The cloud cover over the study area was estimated at ~16.3%, but most of our sample plots were unaffected. The pairs exhibited good horizontal geo-positioning accuracy. The panchromatic (PAN) resolution of the images was 50 cm, while the multispectral image resolution was 2.0 m. The four multispectral bands present were blue (445–517 nm), green (507–586 nm), red (626–696 nm) and near-IR1 (765–899 nm).

We generated point clouds by automatic matching of satellite image pairs. This was done by using the 'DSM extractor' add-on module in ERDAS IMAGINE Photogrammetry Suite (version 16.7.0). The module uses semi global matching (SGM) algorithm

Table 2. Salient ALS data related acquisition parameters.

Parameter	Value
Instrument used	Riegl VQ-1560II S2222736/RiACQUIRE
Aircraft altitude (from mean terrain level)	2100 m
Pulse repetition frequency	1,338,000 Hz
Beam divergence	0.25 mrad
Scanning angle	±20°
Average point density	5.1 pulses/m^2
Side overlap	20%
Num. returns recorded per pulse (max.)	7

(Hirschmüller 2005) to match pixels and thus generate point clouds. Prior to this, the standard procedure of bundle block adjustment with automatic-generated tie points was used to revise the external orientation parameters obtained from the rational polynomial coefficient (RPC) files. The panchromatic images were used to generate a relatively dense point cloud (6.55 points per square metre). The multispectral images were used to generate a relatively sparse multispectral point cloud (0.27 points per square metre). Each point in it had colour intensities of red, green, blue and near-infrared associated with it. We did not use ground control points (GCPs) as part of this procedure as we wanted our methodology to be extended to remote regions in the boreal zone, where the collection of such GCPs may be infeasible. The images were also orthorectified using a globally available 12 m-resolution TanDEM-X DTM (Zink et al. 2021). This was also done without using GCPs.

2.4. Extraction of predictive metrics

In this study, the area-based approach (Næsset 2002) was used to create models of forest attributes. Hence, predictive metrics were extracted from field plots. Metrics were extracted over each of the 33 plots using a 15 m radius buffer from plot centre. We considered three remote sensing feature groups in this study. These groups represent various scenarios of the availability of remote sensing datasets for a new geographic area where our fuel load mapping models are to be applied. These groups are:

(1) ALS only: Up-to-date and high-quality ALS data is available.
(2) Stereo satellite image point cloud data, normalized by DTM: This feature group represents a location where high-resolution stereo satellite data is available, along with a good-quality DTM. It will henceforth be called 'normalized satellite-based point cloud' (NSPC).
(3) Stereo satellite image only: This represents a remote location in the boreal zone, where no ALS or good-quality DTM is available. This feature group will henceforth be called 'satellite data only' (SDO), to underline the fact that it is stand-alone and DTM independent data, that can be derived solely from the high-resolution satellite images.

2.4.1. ALS only

We derived several metrics related to the height (z) and the horizontal (x, y) distribution of points using the lidR package (Roussel et al. 2020). We formed three return categories based on the return number and the total number of returns for that emitted pulse. We term these as 'first' (either be a single return or first-of-many), 'intermediate' (i.e. there are more than two returns and it is neither the first or last return), and 'last' returns (last-of-many; there is more than one return, and it is the last). Metrics were derived separately from each such echo category (Table 3).

2.4.2. NSPC feature group

For this, the panchromatic satellite stereo-imagery-based point cloud was normalized to heights above the ground. This was done by using an ALS-based DTM from the national land survey of Finland. Thus, all height (z) values in the resulting point cloud were with

Table 3. Summary of point cloud metrics derived from ALS data.

Metric	Description
$mean_z$, sd_z, $skew_z$, $kurt_z$, ent_z	The mean, standard deviation, skewness, kurtosis and entropy of z values
$p5_z$, $p10_z$, $p15_z$, …	Percentile (quantile) of height distribution (z values). For example, $p5_z$ is the 5% quantile.
$d1_z$, $d2_z$, … $d10_z$	Density metrics. Cumulative percentage of return in the i^{th} layer according to Woods, Lim, and Treitz (2008).
$mean_{fz}$, sd_{fz}, $skew_{fz}$, $kurt_{fz}$, ent_{fz}, $p95_{fz}$ … etc …	The mean, the standard deviation, skewness, kurtosis, entropy, height percentiles and density metrics of the first returns. Likewise, these statistics were also calculated for the other two return categories; i.e. intermediate returns (e.g. $mean_{iz}$) and last returns (e.g. $mean_{lz}$).
$eigen_{largest}$, $eigen_{medium}$, $eigen_{smallest}$, curvature, linearity, planarity, sphericity, anisotropy, horizontality	This is a set of eigenvalue-based features described in Lucas et al. (2019). These are also calculated for the first, intermediate and last returns.
ri	Rumple index (Jenness 2004). Computes the roughness of a surface as the ratio between its area and its projected area on the ground. For calculating this, a delaunay triangulation of the points is done, and the area of each triangle is computed. This is also calculated for the first, intermediate and last returns.
ULCD	Quantifies the number of returns from the understory, relative to the ground (Wing et al. 2015). In our cause, ground points are assumed to be in the height bin of z_{min} and z_{min} +1.0 m, where z_{min} is associated with the lowest height point in the plot. Likewise, understory points are assumed to be between z_{min} +1.0 m and z_{min} +3.0 m.

respect to the local ground level. From this point cloud, we computed several metrics. The set of derived metrics were similar to those from ALS data (Table 3), except that those based on return categorization (e.g. first return based) were excluded.

2.4.3. SDO feature group

These metrics were derived from the satellite stereo-imagery-based point cloud, without the use of an external DTM.

2.4.3.1. Point cloud-based metrics. These sets of derived metrics were similar to those from ALS data (Table 3), but without return number based categorization. All predictor metrics related to z were computed using standardized z (z_{st}) values. These z_{st} values were computed for each point as:

$$z_{st} = \frac{z_i - \bar{z_p}}{\sigma_{zp}} \tag{1}$$

where z_i is the z coordinate of the point, $\bar{z_p}$ is the average value of z in the plot and σ_{zp} is the standard deviation of z in the plot. This was done based on the recommendation in Giannetti et al. (2018). We also derived several metrics from the multispectral point cloud that factored in the colour intensity of the points (Table 4).

2.4.3.2. Texture related metrics. We computed texture-related metrics from the orthorectified satellite images using the R GLCM package (Zvoleff 2020). For this, we used four image rasters (PAN, red, green, blue) and two derived ones. These were the NDVI and the DSM height rasters; the DSM height was computed from the satellite point cloud. A

Table 4. Various statistics are computed on the set of red colour values associated with the points for every plot-level satellite-based point cloud. Similar statistics are also computed for the blue (e.g. max_b), green (e.g. max_g) and NIR (e.g. max_{nir}) bands.

Metric	Description
max_r, min_r, $mean_r$, sd_r, ske_r, kur_r, ent_r	Maximum, minimum, mean, standard deviation, skewness, kurtosis and entropy.
$iquart1_r$, $iquart2_r$, $iquart3_r$	Quartiles, characterizing the distribution of red intensity values.
$d1_r$, $d2_r$, $d3_r$	Density metrics (four bins).
$i_{red,\ b1,\ min}$, $i_{red,\ b1,\ max}$, etc ...	The point cloud values are first sorted by colour intensity and divided into five equal sized bins (b1...b5). Then, several standard metrics (min, max, percentiles, density metrics) are calculated on the z values in each bin. For example, $i_{red,\ b1,\ mean}$ is the mean z value associated with low (red) intensity points (bin b1).

resolution of 1.0 m was used for the DSM raster, as recommended by Giannetti et al. (2018). The following parameters of the GLCM computation were used:

- Window size (pixels): 9, 13, 17, 21
- Num. grey levels: 2, 5, 10, 20, 30
- Shift parameter: 1, 2, 3

The following textural rasters were computed for each combination of the three parameters above: mean, variance, homogeneity, contrast, dissimilarity, entropy, and second moment. The raster values were aggregated to the plot level using mean and standard deviation (sd). These variations in parameters and types of textural rasters resulted in 7200 values per plot. Variations in parameters were represented by the subscripts associated with the variable name. For example, $tm\_contrast_{\ mean,\ PAN,\ ws=9,\ ngl=5,\ shift=1}$ represents the mean of the contrast texture metric (i.e. tm) of the PAN raster, when the window size (ws) is 9 pixels, the number of grey levels (ngl) is 5 and the shift parameter is 1.

2.4.3.3. Local maxima and minima related metrics.

Metrics derived from the local maxima and minima of the point cloud have been shown to be useful in forest parameter estimations Giannetti et al. (2018). Hence, we computed similar metrics from the DSM raster, which was interpolated from the satellite point cloud (Table 5). Maxima and minima are found in a 3×3cell neighbourhood.

2.4.4. Comparison of vertical profiles of the point clouds

We first visually examined the vertical profiles of the point clouds associated with the stereo satellite data along with the ALS data, along three transects. Three areas of interest

Table 5. Various local maxima and minima-based metrics.

Metric	Description
num_{lmax}	Number of local maxima.
num_{lmin}	Number of local minima.
$mean_{z,\ lmax}$	Mean z value of the local maxima points.
$sd_{z,\ lmax}$	Standard deviation of z value of the local maxima points.
$mean_{z,\ lmin}$	Mean z value of the local minima points.
$sd_{z,\ lmin}$	Standard deviation of z value of the local minima points.
$mean_{slope}$	Mean slope of the CHM.
sd_{slope}	Standard deviation of slope of the CHM.

were identified, which were quite far from each other and generally represented a good sampling of the study area. Transect 1 was in a forested area outside the national park. Transect 2 was also in a fully forested area inside the national park, hence represents natural forests. The associated terrain of these two areas were moderately hilly and was covered with natural conifer forests. The third area (associated with transect 3) was located outside the national park. There was a clearcut area in the northern half, but the rest was forested with mostly old growth forests.

2.4.5. Regression modelling

We formulated several multivariate linear regression models to link continuous field-measured dependent variables and remote sensing explanatory metrics (independent variables). We preferred such regression models as they are robust, amenable to formulation with a relatively small dataset and transparent to interpretation and inference. The dependent variables were:

(1) Dominant height (m)
(2) Foliage biomass (t ha^{-1})
(3) Canopy base height (m)

For the formulation of such models, the following steps were followed. For each dependent variable and feature group, we constructed a set of explanatory variables such that the pairwise correlation of any two of these variables was less than 70%. We also ensured that explanatory variables found useful in previous modelling studies were included in this set, if possible. This was done by adding in any such variable, and then dropping other variables (if required) so as to keep all pairwise correlations below the 70% threshold. Then, we performed an exhaustive search for the best predictor variables from this set using the R 'leaps' package. An additional constraint was that the maximum number of predictor variables allowed was three. We preferred such parsimonious models to minimize the chance of overfitting. Various goodness-of-fit metrics such as R^2, RMSE and relative RMSE (%RMSE) were estimated using all 33 plots. We used the formulas:

$$RMSE = \sqrt{\frac{1}{N}\sum_{i=1}^{N}(\hat{y}_i - y_i)^2} \quad (2)$$

$$\%RMSE = \frac{RMSE \times 100}{\bar{y}} \quad (3)$$

where N is the number of field plots, $\hat{y}_i$is the model predicted value for the i^{th} plot, $y_i$is the field measured value for the i^{th} plot, and $\bar{y}$ is the mean of all $y_i$values. When the models included natural logarithm transformations, the resulting bias in RMSE was corrected for using the method prescribed in Mehtätalo and Lappi (2020).

We also developed logistic regression models to predict understory presence as a categorical variable (two classes: present, absent) from the remote sensing data. The steps were similar to those for the regression models, as outlined above. The overall accuracy of the classification models, the kappa values and the McFadden pseudo R^2 values McFadden (1974) were calculated using all 33 plots.

3. Results

3.1. Comparison of vertical profiles of the point clouds

We first performed a comparative analysis of the vertical structure and distribution of points based on the two sensors at three transect locations (Figure 2). The bare earth portion of transect 3 shows that there is a good vertical co-registration between the two point-clouds (i.e. satellite and ALS based). On closer analysis of these three vertical profiles, several differences between the stereo satellite and ALS point clouds can be seen. A conspicuous difference is that the satellite-based point cloud is mostly concentrated in the upper parts of the forest canopy, and reaches near the ground level only when the vegetation height itself is low. This is in contrast to the ALS based point cloud, which is much more representative of the entire vertical vegetation structure and the ground too. Another general issue with the satellite-based point cloud is that of flattening of tree crown shapes. We measured a vertical difference of as much as 4 m between the ALS and satellite-based point clouds in some parts, caused by this effect. This and other related artefacts result in the omission of several individual trees, as can be seen in the satellite point cloud. One can also see the presence of several gaps and spikes associated with this point cloud. In the case of transect 3, one can also see examples of the satellite point cloud showing vegetation where there is none (as per ALS data).

The general trend of the satellite-based point cloud being skewed towards the upper part of the canopy is clearly seen in the z-values of density plots (Figure 3). Meanwhile, the

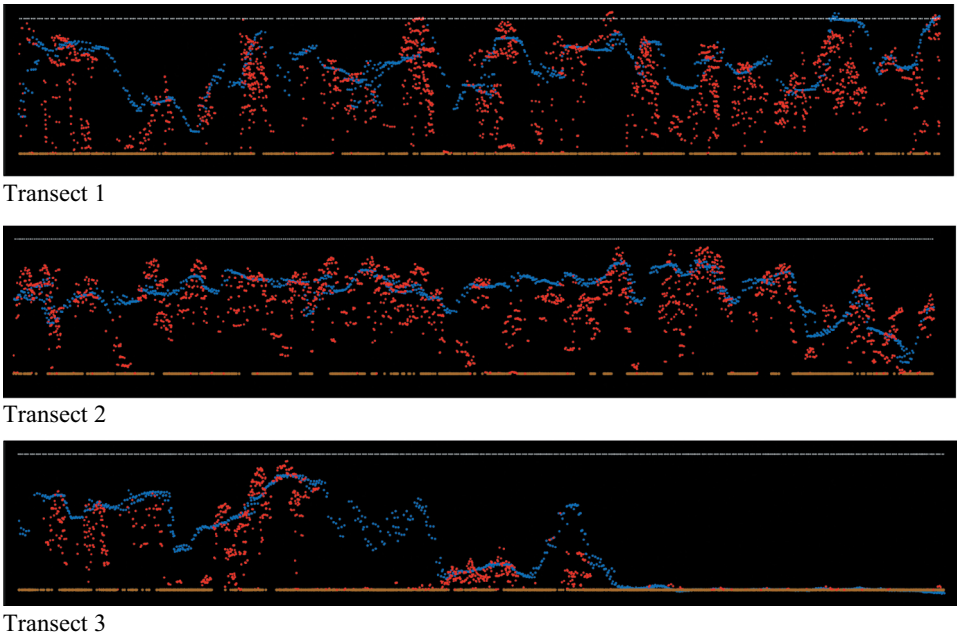

Figure 2. Vertical profile view of three selected transects. The point cloud height above ground is depicted in all of them. Each transect is 170 m in length and ~1 m wide/deep. The blue points represent those from the stereo satellite based point cloud, while the red (vegetation) and brown (ground) points are from the ALS data. The thin, dotted white line at the top is a constant 25 m height marker that has been added in to provide a vertical height reference.

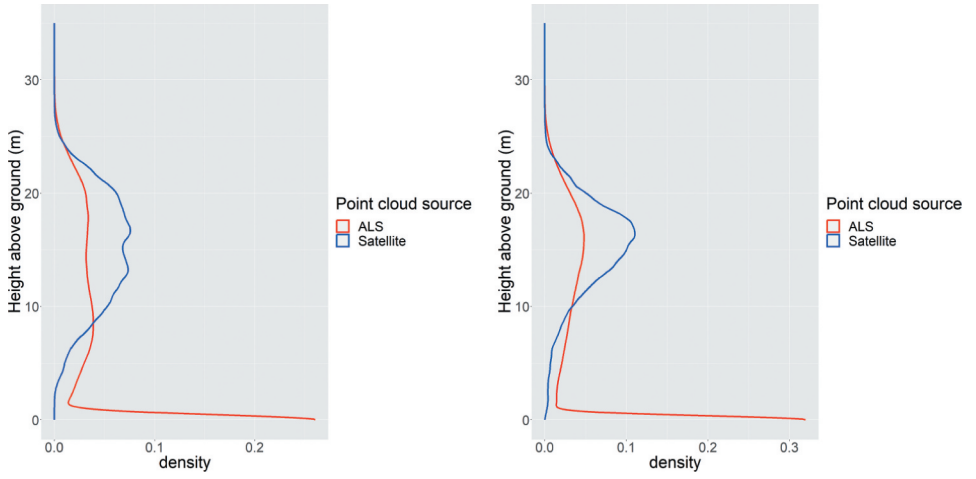

Figure 3. Vertical point densities for the area around the two fully forested transects. These represent the proportion of points in the particular height bin.

Table 6. Percent points for each heigh bin (relative to the ground) for the two forested transects analysed.

	Transect 1		Transect 2	
Height bin (m)	% points, ALS	% points, stereo satellite	% points, ALS	% points, stereo satellite
0 to 5	38.3	1.4	36.2	2.0
5 to 10	18.3	14.4	13.5	8.4
10 to 15	16.7	33.1	20.3	33.6
15 to 20	16.4	35.1	21.6	46.0
20 to 25	9.5	15.6	7.9	9.8
25 to 30	0.9	0.4	0.5	0.1
Total	100.0	100.0	100.0	100.0

density spikes near the ground show the ability of ALS pulses to penetrate the canopy and reach the understory and ground. In general, ALS returns are much more evenly spread along the vertical gradient. The vertical distribution of points in various height bins can be seen in Table 6. The advantage of ALS-based data for sampling the understory and the ground (0-5 m height bin) when compared to stereo image data can be seen clearly here.

3.2. Modeling of forest attributes

We had considered three feature groups, representing different scenarios of availability of remote sensing data (section 2.4). The associated estimated performance statistics of the models formulated are shown in Table 7. The scatterplots of the three continuous variables and the associated adjusted R^2 values can be seen in Figure 4. The maximum variance inflation factor (VIF) value associated with these models was 2.5, which shows that multicollinearity is not a problem. As expected, dominant height is predicted very well with ALS data, with a low RMSE of 0.6 m and a relative RMSE of 2.6%. Predictors based on satellite point cloud data (feature groups NSPC and SDO) also yield relatively low

Table 7. RMSE and relative RMSE (%RMSE) estimated for the four dependent variables for the three feature groups (ALS, NSPC, SDO) considered. The McFadden pseudo R^2, overall accuracy and kappa values are given for the categorical variable of understory presence.

	Dominant height (m)		Foliage biomass (t ha^{-1})		Canopy base height (m)		Understory presence (present/absent)		
	RMSE (m)	%RMSE	RMSE (t ha^{-1})	%RMSE	RMSE (m)	%RMSE	R^2	Overall accuracy	Kappa
ALS	0.6	2.6%	1.85	23.9%	0.98	14.1%	0.57	91%	0.8
NSPC	1.55	6.6%	2.35	30.3%	1.0	14.3%	0.12	69.7%	0.25
SDO	2.6	11%	2.32	30%	1.18	16.9%	0.37	78.8%	0.51

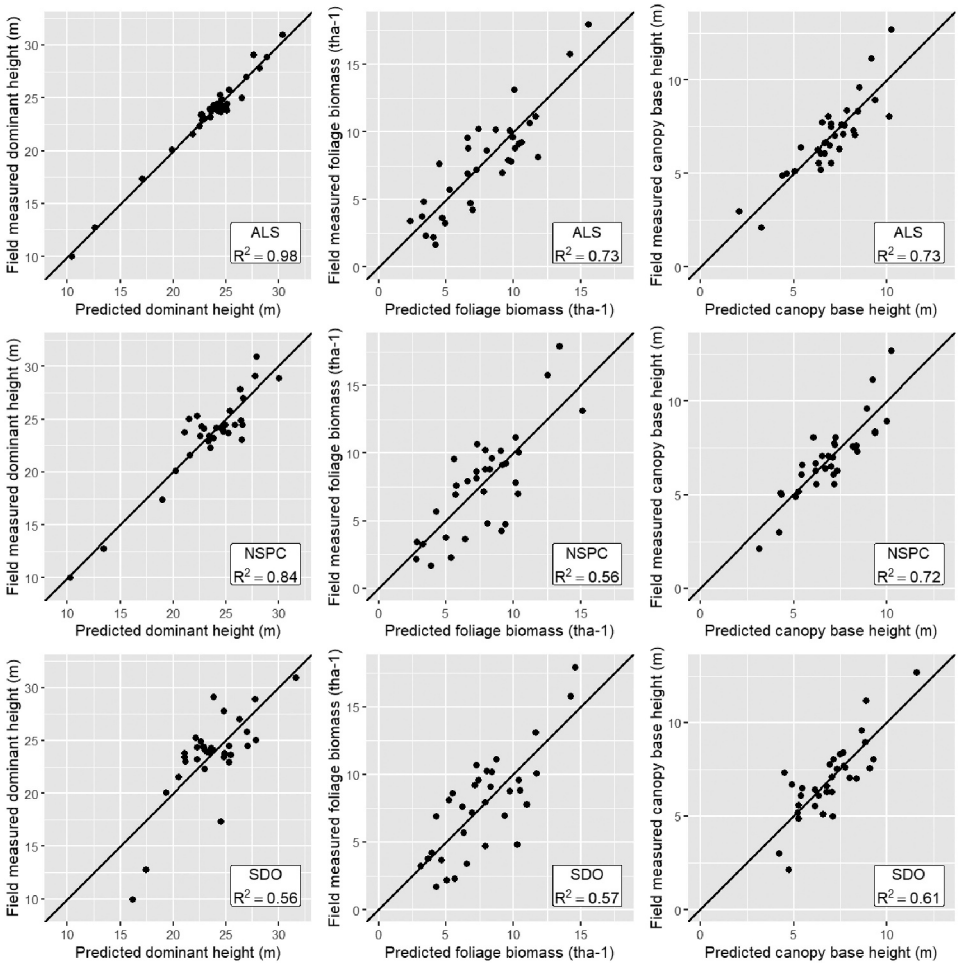

Figure 4. Scatterplot showing the predicted values of our formulated models against the field measured ones, for three continuous forest parameter variables. The goodness of fit of the models is indicated by the adjusted R^2 value inside the plot.

RMSEs for this dependent variable, below 2.2 m. Foliage biomass is predicted reasonably well by all three feature groups, with a relative RMSE ranging from 24 to 30%, but with adjusted R^2 values ranging from 0.56 to 0.72. The prediction of canopy base height follows

a pattern similar to dominant height, with ALS case yielding the best results (RMSE of 0.98 m) and the SDO case the least accurate (RMSE of 1.15 m). Understory presence is predicted very well with ALS data (91% accuracy). The prediction accuracy is good with SDO features, but poor with satellite point cloud data normalized by ALS (NSPC features).

3.3. Predictor variables

The variables that were selected as predictors as a result of the correlation-based screening and the exhaustive search can be seen in Table 8. The correlation values given independently bring out their efficacy in predicting the dependent variable, in addition to being selected for the final model. It can be seen that the first, intermediate and last returns are especially useful in the ALS feature group case. For ALS-based foliage biomass, an eigen value based metric ($eigen_{largest,iz}$) was selected and so was a metric that quantifies the roughness of the first returns surface (rumple index; ri_{fz}). Density-based metrics ($d5_{fz}$, $d9_{lz}$, $d9_{iz}$) were also prominent predictors for this feature group. For the NSPC feature group, the dominant height was predicted well with a univariate model based on the 95th height percentile. Fair prediction accuracies were seen for foliage biomass and crown base height, and the chosen predictor variables were similar to those chosen for the respective ALS case. Understory presence prediction was poor (kappa value of 0.25) and rather weak models could only be formulated for this dependent variable. As for the SDO feature group, texture metric based variables play an important role in three of the four models formulated. These may be either based on the GLCM texture measure of second moment ($tm\_second\_moment_{sd,\ DSM,\ ws=9,\ ngl=30,\ shift=3}$) or contrast ($tm\_contrast_{mean,\ NDVI,\ ws=13,\ ngl=5,\ shift=2}$) or, etc. Also, the raster on which the texture was computed could be different; for example, PAN ($tm\_correlation_{mean,\ PAN,\ ws=13,\ ngl=30,\ shift=3}$) or NDVI ($tm\_contrast_{mean,\ NDVI,\ ws=13,\ ngl=5,\ shift=2}$). Three such texture metrics were based on the 1.0 m DSM raster (e.g. two in the dominant height

Table 8. Predictor variables that were used in the formulated linear regression models for the three feature groups. All variables were significant at the p-value level of 0.05 except in two cases where strong models could not be achieved (indicated below). The percentage value in the parenthesis next to each variable indicates its correlation to the dependent variable. In the case of understory presence, the binary categorical dependent variable is coded as a numerical value (1 or 0) for calculating this correlation value.

	Dominant height (m)	Foliage biomass (t ha^{-1})	Canopy base height (m)	Understory presence (present/absent)
ALS	$p95_{fz}$ (98%), $skew_{fz}$ (26%)	$skew_{lz}$ (67.6%), ri_{fz} (47.4%), $eigen_{largest,iz}$ (10.6%)	$d5_{fz}$ (80.6%), $p90_{fz}$ (55.9%), $skew_{lz}$ (5.4%)	$d9_{lz}$ (62.7%), $d9_{iz}$ (60.3%)
NSPC	$p95_z$ (88%)	$p95_z$ (64%), $eigen_{medium}$ (46%), $skew_z$ (23%)	$p95_z$ (64%), sd_z (44%) $skew_z$ (9%)	$p20_z$ (p-value = 0.13) (33%), $d9_z$ (p-value = 0.327) (28%)
SDO	$tm\_second\_moment_{sd,\ DSM,\ ws=9,\ ngl=30,\ shift=3}$ (55%), $tm\_correlation_{mean,\ PAN,\ ws=13,\ ngl=30,\ shift=3}$ (45%), $tm\_second\_moment_{mean,\ DSM,\ ws=9,\ ngl=2,\ shift=3}$ (26%)	$tm\_contrast_{mean,\ NDVI,\ ws=13,\ ngl=5,\ shift=2}$ (56%), $eigen_{medium}$ (55%), $i_{red,\ b5,\ d2}$ (24%)	$tm\_variance_{mean,\ DSM,\ ws=21,\ ngl=30,\ shift=1}$ (60%), $kurt_z$ (49%), $i_{blue,\ b5,\ d3}$ (36%)	$i_{green,\ b5,\ d3}$ (43%), ULCD (31%), num_{lmax} (17%)

prediction model) and hence quantified the canopy surface undulation and related properties of the point cloud.

A metric based on the colour intensity of the multispectral point cloud ($i_{red, b5, d2}$) was found to be useful for predicting foliage biomass. In this case, bin 'b5' represents high red intensity points (b1 is the lowest red intensity, and b5 is the highest). Hence, this metric quantifies an aspect of the z value distribution (i.e. the d1 density metric) of high red intensity points in the plot. This also suggests in general that the distribution of high red intensity points is an indication of the foliage biomass on the plot. The choice of such metrics in three instances of the SDO feature group indicates the utility of the multispectral point cloud for vegetation parameter estimation.

4. Discussion

In this study, we examined the ability of high-resolution stereo satellite-based remote sensing data to characterize various boreal forest fire-related fuel load parameters, and contrast it as a possible alternative to ALS data. We considered the prediction of dominant height, foliage biomass, canopy base height and understory presence using three distinct feature groups as predictors. The estimated model performance statistics using ALS data (see Table 7 and Figure 4) were similar when compared to previous studies (e.g. see Maltamo et al. (2020) and Zolkos, Goetz, and Dubayah (2013) for crown biomass, Maltamo et al. (2020) for canopy base height). Understory presence is also well-predicted with ALS data: the estimated McFadden R^2 value of 0.57 indicates a very good fit and while a kappa value of 0.8 is considered as substantial agreement between model predicted and observed classes. The associated R^2 is similar to those obtained by a study about the detection of sub-canopy vegetation using ALS data in boreal forests (Jarron et al. 2020). The NSPC feature group represents the ability of the stereo satellite-based point cloud to capture the three dimensional features of vegetation (i.e. contrast it to that captured by the ALS point cloud). Thus, the orthoimage-based multispectral information component was omitted in this case. The goodness of fit of prediction models for above ground biomass from similar WorldView-2 stereo satellite data for temperate forests was comparable to ours (Fassnacht et al. 2017). In that case, the R^2 was 0.64 and the %RMSE was 24.9%. The relative RMSE of prediction of above ground biomass was in the order of 20–30% using WorldView-2 stereo-imagery for a similar study area (Vastaranta et al. 2018). Meanwhile, better goodness of fit values were reported by Wittke et al. (2019) for the same satellite, the R^2 values were between 0.66 and 0.87 and %RMSE values between 7.9 and 17.3%. Visual examination of the stereo satellite point cloud in our case had shown that it is a more approximate representation of canopy structure, compared to ALS data (Figure 2). This observation is supported by further analysis of the vertical distribution of stereo satellite points (Figure 3 and Table 6). Similar stereo satellite-based tree detection studies in relatively sparse forests had produced poor results, with only 8–9% tree detection rate (Goldbergs et al. 2019). Individual tree height is usually underestimated by stereo satellite point cloud data (Goldbergs 2021, Table 5); it is further reported there that such underestimation can be up to several metres, or 8% of mean canopy height in some cases. Hence as expected, the associated performance statistics of our NPSC models are lower than those of ALS. Nevertheless, the satellite point cloud does capture the general rough envelope and height profile of the top of the canopy, albeit with a

significant bias. Hence, it may be suitable for some level of operational use. Understory presence is not well predicted in this case: the kappa value of 0.25 indicates 'none to slight' agreement. This is a consequence of very poor sampling below 5 m height threshold (see Table 6).

The SDO feature group represents the case where a high-quality DTM is not available for normalization of the stereo satellite point cloud. Hence, predictor variables are derived solely from the satellite data. Interestingly, we were able to formulate a reasonably accurate model for the prediction of dominant height, purely based on such satellite image data (adjusted R2 value of 0.56, RMSE of 11%). A recent effort combining high-resolution spaceborne lidar sampling data with Landsat images generated global canopy height maps at 30 m resolution; the associated R2 values were ≈ 0.61 (Potapov et al. 2021) which compares closely with ours. The RMSE reported there was ~9 m, when compared to reference ALS data. All of our chosen predictors in the SDO case had good correlation with the response variable (up to 55%) and were statistically significant in the prediction models (at the 0.02 level). Canopy height is a good indicator of terrestrial ecosystem functioning and aboveground carbon stock, and it is ranked as a priority variable to be observed via satellites (Skidmore et al. 2021). In the forestry context, it is well established that there is high correlation between such heights and growing stock (Pretzsch 2009). Canopy base height is also predicted reasonably well, the associated RMSE is ~17%. Foliage biomass prediction is less accurate, with RMSE in the order of 30%. The error statistics for these three variables are similar to the 15–20% RMSE range reported by Giannetti et al. (2018), who used a similar DTM-independent approach to derive forest volume from unoccupied aerial vehicle (UAV) data. Meanwhile, the kappa value for understory presence estimation in the SDO case implies that there is only moderate agreement between the predicted and observed classes.

As part of the modelling effort, we identified several variables for all three feature groups that could be used for the prediction of forest fire related biophysical parameters over large areas. Most variables that were selected for the first feature group (ALS data only) were quite similar to those selected as part of other studies. For example, a similar recent study found that the 95th percentile and skewness of ALS first returns are important in estimation of forest fuel load parameters (Maltamo et al. 2020). We also picked four eigenvalue-based metrics. These are not that common in forestry but have been used in ecology-related studies (Koma, Seijmonsbergen, and Kissling 2021; Rosier et al. 2021). A relatively strong model for dominant height could be formulated for the NSPC feature group (RMSE of 1.55 m, relative RMSE of 6.6%). This result differs from a previous study where a high relative RMSE of 44.4% was reported for growing stock in Bavarian forests for WorldView-2-based point cloud, normalized using an ALS DTM (Straub et al. 2013). As for the SDO feature group, we observed that all the four models formulated had a combination of at least one spectral predictor variable (e.g. $tm\_correlation_{mean,\ PAN,\ ws=13,\ ngl=30,\ shift=3}$ in the dominant height model) and a structural height based one (e.g. $tm\_second\_moment_{sd,\ DSM,\ ws=9,\ ngl=30,\ shift=3}$ in the dominant height model). This is in agreement with the conclusions of Immitzer et al. (2016), who found it was useful to combine predictor variables that represented spectral and height information into models. For all three feature groups, the presence of understory is predicted by canopy and overstory-related metrics such as $d9_{lz}$, $p20_{z}$ and $i_{green,\ b5,\ d3}$. This is in agreement to similar studies, where metrics

related to overstory variability and distribution were found to be good predictors (Jarron et al. 2020; Maltamo et al. 2020). We also found that the ULCD metric is useful in predicting understory presence. This metric tries the quantify the number of points in the understory bin, relative to the ground bin. Other studies have also demonstrated its utility in detection of understory presence (Gopalakrishnan et al. 2018; Wing et al. 2015).

Several authors have presented their research findings of using very high-resolution stereo satellite imagery normalized by a good-quality DTM (Liu et al. 2021; Straub et al. 2013; Ullah et al. 2020; Vastaranta et al. 2018). But a significant drawback of such an approach is the requirement of such a DTM, which may not be available in many areas. A prominent near-global DEM product that has been used in many studies is the Shuttle Radar Topography Mission (SRTM); but it has significant bias in vegetated areas (so-called 'vegetation bias') (O'Loughlin et al. 2016). A study by Rodriguez, Morris, and Belz (2006) using ground control points estimated the errors in associated verticals height were in the order of 8 m. Similar issues are also associated with the TanDEM-X-based DTM product (Rizzoli et al. 2017). Another alternative is trying to extract a DTM from the satellite-based point cloud itself, as is done with ALS data. This can theoretically be done by identifying and filtering out ground points, assuming that they would sample the terrain morphology sufficiently. For a similar approach with unmanned aerial vehicle (UAV) based point clouds, see Miller et al. (2017). But the percentage of stereo satellite points at the ground level is very low for us (Table 6). Hence, it is infeasible in our case. Taking all these into consideration, the calculation of predictors without a normalizing DTM (as we have done for the SDO feature group) is an interesting possibility. We found that the RMSE and relative RMSEs of the associated models were in the range of those of the other feature groups. The intuition behind this result is roughly the same as that behind why manual photointerpretation of forest stand height is so effective (error typically less than 1 m in some cases; see Tompalski et al. (2021)). We also identified several DTM-independent predictor variables that were well-correlated (50–60% correlation) with plot-level forest parameters (Table 8). Metrics based on the texture of either the orthorectified satellite image or the DSM were used at least once in each of the four models thus formulated. Texture metrics from the orthorectified images of similar satellites that quantify the spectral variance at the top of the forest canopy have been found useful before (Eckert 2012; Immitzer, Atzberger, and Koukal 2012; Li et al. 2022). The selection of DSM raster-based textural variables as predictor variables in two instances (for example, $\text{tm\_second\_moment}_{\text{sd, DSM, ws = 9, ngl = 30, shift = 3}}$) is in agreement with other studies that had arrived at similar findings (Bohlin, Wallerman, and Fransson 2012; Niemi and Vauhkonen 2016). But it should be kept in mind that a number of factors including the base-to-height (B/H) ratio, image acquisition geometry (both sun-to-sensor and sensor-to-target) and species-specific canopy structure and composition govern the completeness and vertical accuracy of the image-based DSM point cloud (Goldbergs 2023) from which many of these metrics were derived. Hence, associated forest parameter prediction models developed in one context (study area, sensor, image acquisition geometry, etc.) cannot be assumed to generalize reliably to another. We also note that the

presence of clouds (including translucent ones and cloud wisps), cloud shadows and atmospheric haze remain a challenge with such satellite-based systems. But it is expected that this problem will be partly alleviated by the increase in the number and manoeuvrability of such satellites.

The results of this study have the following implications: (1) ALS data is highly suitable for estimation and mapping of several forest fire related fuel load parameters (e.g. RMSEs range from 2.6–23.9%), (2) Normalized satellite-based point cloud (NSPC) data is less suitable for such purposes due to the presence of bias and several artefacts. It is not suitable for understory presence detection; the associated classifier performance statistics are poor, (3) The combined use of both vegetation spectral and structural information in the SDO feature group yields performance statistics comparable to that of ALS. Spectral texture-related information is well correlated with several forest parameters, including understory presence. Thus, there seems to be potential in using solely such information (i.e. no high-quality auxiliary DTM needed) for forest fuel load estimation in isolated boreal areas. This indicates that datasets of various important forest parameters may be derived from such stereo satellite data. Such additional ability to frequently monitor forests in remote areas are of increasing importance for the coming years, given that there are wide-ranging concerns about global forest health and resilience (Forzieri et al. 2022; Seidl et al. 2017).

5. Conclusions

The results of this study show that fairly accurate maps of various important forest parameters related to wildfires can be made using very high resolution optical satellite data coupled with field measurements. We confirmed the usefulness of various texture-related parameters (both derived from the DSM or from the multispectral orthorectified image) that had been previously reported in the literature. Dominant height and canopy base height were associated with better prediction accuracies (RMSE between 11% and 17%) while foliage biomass was not so well predicted (RMSE ~30%). Our findings indicate that high resolution optical satellites have the potential to aid in the estimation of large area forest parameter estimation even over areas lacking a high-quality DTM. Further research involving a larger and more heterogeneous study area and a larger set of forest plots is needed. Better characterization of the effect of varied acquisition and illumination geometries of images is also needed. In conclusion, our findings cast a promising light on the prospect of using stereo-image capable high resolution optical satellite to produce and update forest parameter maps.

Acknowledgements

We wish to express our gratitude to the European space agency (ESA) and European Space Imaging (EUSI) for providing the high-resolution commercial satellite images used for this research.

Disclosure statement

No potential conflict of interest was reported by the author(s).

Funding

This work was supported by the Research Council of Finland under grant numbers [337127] & p337655] (part of the UNITE flagship project, see https://uniteflagship.fi/.) and the project Asynchronous Datasets in Large-Area Forest Inventories by Remote Sensing [grant number 355267].

ORCID

Ranjith Gopalakrishnan http://orcid.org/0000-0002-0788-8407
Lauri Korhonen http://orcid.org/0000-0002-9352-0114
Petteri Packalen http://orcid.org/0000-0003-1804-0011

Data availability statement

The data supporting the findings of this study are available from the corresponding author upon reasonable request.

References

Bohlin, J., J. Wallerman, and J. E. S. Fransson. 2012. "Forest Variable Estimation Using Photogrammetric Matching of Digital Aerial Images in Combination with a High-Resolution DEM." *Scandinavian Journal of Forest Research* 27 (7): 692–699. https://doi.org/10.1080/02827581.2012.686625.

Bousfield, C. G., D. B. Lindenmayer, and D. P. Edwards. 2023. "Substantial and Increasing Global Losses of Timber-Producing Forest Due to Wildfires." *Nature Geoscience* 16 (12): 1145–1150. https://doi.org/10.1038/s41561-023-01323-y.

Chirici, G., R. Scotti, A. Montaghi, A. Barbati, R. Cartisano, G. Lopez, M. Marchetti, R. E. McRoberts, H. Olsson, and P. Corona. 2013. "Stochastic Gradient Boosting Classification Trees for Forest Fuel Types Mapping Through Airborne Laser Scanning and IRS LISS-III Imagery." *International Journal of Applied Earth Observation and Geoinformation* 25:87–97. https://doi.org/10.1016/j.jag.2013.04.006.

Clarke, H., R. H. Nolan, V. Resco De Dios, R. Bradstock, A. Griebel, S. Khanal, and M. M. Boer. 2022. "Forest Fire Threatens Global Carbon Sinks and Population Centres Under Rising Atmospheric Water Demand." *Nature Communications* 13 (1): 7161. https://doi.org/10.1038/s41467-022-34966-3.

Duane, A., M. Castellnou, and L. Brotons. 2021. "Towards a Comprehensive Look at Global Drivers of Novel Extreme Wildfire Events." *Climatic Change* 165 (3): 43. https://doi.org/10.1007/s10584-021-03066-4.

Eckert, S. 2012. "Improved Forest Biomass and Carbon Estimations Using Texture Measures from WorldView-2 Satellite Data." *Remote Sensing* 4 (4): 810–829. https://doi.org/10.3390/rs4040810.

Fassnacht, F. E., D. Mangold, J. Schäfer, M. Immitzer, T. Kattenborn, B. Koch, and H. Latifi. 2017. "Estimating Stand Density, Biomass and Tree Species from Very High Resolution Stereo-Imagery–Towards an All-In-One Sensor for Forestry Applications?" *Forestry: An International Journal of Forest Research* 90 (5): 613–631. https://doi.org/10.1093/forestry/cpx014.

Fassnacht, F. E., J. C. White, M. A. Wulder, and E. Næsset. 2024. "Remote Sensing in Forestry: Current Challenges, Considerations and Directions." *Forestry: An International Journal of Forest Research* 97 (1): 11–37. https://doi.org/10.1093/forestry/cpad024.

Forzieri, G., V. Dakos, N. G. McDowell, A. Ramdane, and A. Cescatti. 2022. "Emerging Signals of Declining Forest Resilience Under Climate Change." *Nature* 608 (7923): 534–539. https://doi.org/10.1038/s41586-022-04959-9.

Gajardo, J., M. García, and D. Riaño. 2014. "Applications of Airborne Laser Scanning in Forest Fuel Assessment and Fire Prevention." In *Forestry Applications of Airborne Laser Scanning*, edited by M. Maltamo, E. Næsset, and J. Vauhkonen, 439–462. Vol. 27. Dordrecht: Springer Netherlands. https://doi.org/10.1007/978-94-017-8663-8_22.

Gale, M. G., G. J. Cary, A. I. Van Dijk, and M. Yebra. 2021. "Forest Fire Fuel Through the Lens of Remote Sensing: Review of Approaches, Challenges and Future Directions in the Remote Sensing of Biotic Determinants of Fire Behaviour." *Remote Sensing of Environment* 255:112282. https://doi.org/10.1016/j.rse.2020.112282.

Giannetti, F., G. Chirici, T. Gobakken, E. Næsset, D. Travaglini, and S. Puliti. 2018. "A New Approach with DTM-Independent Metrics for Forest Growing Stock Prediction Using UAV Photogrammetric Data." *Remote Sensing of Environment* 213:195–205. https://doi.org/10.1016/j.rse.2018.05.016.

Goldbergs, G. 2021. "Impact of Base-to-Height Ratio on Canopy Height Estimation Accuracy of Hemiboreal Forest Tree Species by Using Satellite and Airborne Stereo Imagery." *Remote Sensing* 13 (15): 2941. https://doi.org/10.3390/rs13152941.

Goldbergs, G. 2023. "Comparison of Canopy Height Metrics from Airborne Laser Scanner and Aerial/Satellite Stereo Imagery to Assess the Growing Stock of Hemiboreal Forests." *Remote Sensing* 15 (6): 1688. https://doi.org/10.3390/rs15061688.

Goldbergs, G., S. W. Maier, S. R. Levick, and A. Edwards. 2019. "Limitations of High Resolution Satellite Stereo Imagery for Estimating Canopy Height in Australian Tropical Savannas." *International Journal of Applied Earth Observation and Geoinformation* 75:83–95. https://doi.org/10.1016/j.jag.2018.10.021.

Gopalakrishnan, R., L. Korhonen, M. Maltamo, S. Adnan, and P. Packalen. "Prediction and Mapping of Boreal Forest Fire Fuel Loads Using High-Resolution Satellite Stereo Imagery." Accessed September 2, 2025. https://ssrn.com/abstract=4867837.

Gopalakrishnan, R., V. A. Thomas, R. H. Wynne, J. W. Coulston, and T. R. Fox. 2018. "Shrub Detection Using Disparate Airborne Laser Scanning Acquisitions Over Varied Forest Cover Types." *International Journal of Remote Sensing* 39 (4): 1220–1242. https://doi.org/10.1080/01431161.2017.1399476.

Hirschmüller, H. 2005. "Accurate and Efficient Stereo Processing by Semi-Global Matching and Mutual Information." *2005 IEEE Computer Society Conference on Computer Vision and Pattern Recognition (CVPR'05)*, San Diego, CA, USA. Vol. 2. 807–814. https://ieeexplore.ieee.org/abstract/document/1467526/.

Immitzer, M., C. Atzberger, and T. Koukal. 2012. "Tree Species Classification With Random Forest Using Very High Spatial Resolution 8-Band WorldView-2 Satellite Data." *Remote Sensing* 4 (9): 2661–2693. https://doi.org/10.3390/rs4092661.

Immitzer, M., C. Stepper, S. Böck, C. Straub, and C. Atzberger. 2016. "Use of WorldView-2 Stereo Imagery and National Forest Inventory Data for Wall-to-Wall Mapping of Growing Stock." *Forest Ecology & Management* 359:232–246. https://doi.org/10.1016/j.foreco.2015.10.018.

Jarron, L. R., N. C. Coops, W. H. MacKenzie, P. Tompalski, and P. Dykstra. 2020. "Detection of Sub-Canopy Forest Structure Using Airborne LiDAR." *Remote Sensing of Environment* 244:111770. https://doi.org/10.1016/j.rse.2020.111770.

Jenness, J. S. 2004. "Calculating Landscape Surface Area from Digital Elevation Models." *Wildlife Society Bulletin* 32 (3): 829–839. https://doi.org/10.2193/0091-7648(2004)032[0829:CLSAFD]2.0.CO;2.

Koma, Z., A. C. Seijmonsbergen, and W. D. Kissling. 2021. "Classifying Wetland-Related Land Cover Types and Habitats Using Fine-Scale Lidar Metrics Derived from Country-Wide Airborne Laser Scanning." *Remote Sensing in Ecology and Conservation* 7 (1): 80–96. https://doi.org/10.1002/rse2.170.

Kukkonen, M., M. Maltamo, and P. Packalen. 2017. "Image Matching as a Data Source for Forest Inventory–Comparison of Semi-Global Matching and Next-Generation Automatic Terrain Extraction Algorithms in a Typical Managed Boreal Forest Environment." *International Journal of Applied Earth Observation and Geoinformation* 60:11–21. https://doi.org/10.1016/j.jag.2017.03.012.

Labenski, P., M. Ewald, S. Schmidtlein, and F. Ewald Fassnacht. 2022. "Classifying Surface Fuel Types Based on Forest Stand Photographs and Satellite Time Series Using Deep Learning." *International Journal of Applied Earth Observation and Geoinformation* 109:102799. https://doi.org/10.1016/j.jag.2022.102799.

Lehtonen, I., A. Venäläinen, M. Kämäräinen, H. Peltola, and H. Gregow. 2016. "Risk of Large-Scale Fires in Boreal Forests of Finland Under Changing Climate." *Natural Hazards and Earth System Sciences* 16 (1): 239–253. https://doi.org/10.5194/nhess-16-239-2016.

Li, Y., R. Chen, B. He, and S. Veraverbeke. 2022. "Forest Foliage Fuel Load Estimation from Multi-Sensor Spatiotemporal Features." *International Journal of Applied Earth Observation and Geoinformation* 115:103101.

Liu, X., J. Frey, M. Denter, K. Zielewska-Büttner, N. Still, and B. Koch. 2021. "Mapping Standing Dead Trees in Temperate Montane Forests Using a Pixel-and Object-Based Image Fusion Method and Stereo WorldView-3 Imagery." *Ecological Indicators* 133:108438. https://doi.org/10.1016/j.ecolind.2021.108438.

Lucas, C., W. Bouten, Z. Koma, W. D. Kissling, and A. C. Seijmonsbergen. 2019. "Identification of Linear Vegetation Elements in a Rural Landscape Using LiDAR Point Clouds." *Remote Sensing* 11 (3): 292. https://doi.org/10.3390/rs11030292.

Maltamo, M., T. Karjalainen, J. Repola, and J. Vauhkonen. 2018. "Incorporating Tree-and Stand-Level Information on Crown Base Height into Multivariate Forest Management Inventories Based on Airborne Laser Scanning." *Silva Fennica* 52 (3): 3. https://doi.org/10.14214/sf.10006.

Maltamo, M., and P. Packalen. 2014. "Species-Specific Management Inventory in Finland." In *Forestry Applications of Airborne Laser Scanning*, edited by M. Maltamo, E. Næsset, and J. Vauhkonen, 241–252. Dordrecht, Netherlands: Springer. https://link.springer.com/content/pdf/10.1007/978-94-017-8663-8.pdf .

Maltamo, M., J. Räty, L. Korhonen, E. Kotivuori, M. Kukkonen, H. Peltola, J. Kangas, and P. Packalen. 2020. "Prediction of Forest Canopy Fuel Parameters in Managed Boreal Forests Using Multispectral and Unispectral Airborne Laser Scanning Data and Aerial Images." *European Journal of Remote Sensing* 53 (1): 245–257. https://doi.org/10.1080/22797254.2020.1816142.

Martin-Ducup, O., J.-L. Dupuy, M. Soma, J. Guerra-Hernandez, E. Marino, P. M. Fernandes, A. Just, J. Corbera, M. Toutchkov, and C. Sorribas. 2025. "Unlocking the Potential of Airborne LIDAR for Direct Assessment of Fuel Bulk Density and Load Distributions for Wildfire Hazard Mapping." *Agricultural and Forest Meteorology* 362:110341. https://doi.org/10.1016/j.agrformet.2024.110341.

McFadden, D. 1974. "Conditional Logit Analysis of Qualitative Choice Behavior." In *Frontiers in Econometrics*, edited by P. Zarembka, 105–142. New York: Academic Press. https://escholarship.org/content/qt61s3q2xr/qt61s3q2xr.pdf .

Mehtätalo, L., and J. Lappi. 2020. *Biometry for Forestry and Environmental Data: With Examples in R*. Boca Raton, FL, USA: Chapman and Hall/CRC.

Miller, E., J. P. Dandois, M. Detto, and J. S. Hall. 2017. "Drones as a Tool for Monoculture Plantation Assessment in the Steepland Tropics." *Forests* 8 (5): 168. https://doi.org/10.3390/f8050168.

Næsset, E. 2002. "Predicting Forest Stand Characteristics with Airborne Scanning Laser Using a Practical Two-Stage Procedure and Field Data." *Remote Sensing of Environment* 80 (1): 88–99. https://doi.org/10.1016/S0034-4257(01)00290-5.

National land survey of Finland. 2023. "Laser Scan Service 2023 (Details of Contracts Awarded, in Finnish). Reference Number: MML 30774/02." Accessed September 2, 2025. https://www.hankintailmoitukset.fi/en/public/procurement/69075/notice/114751/overview.

Niemi, M. T., and J. Vauhkonen. 2016. "Extracting Canopy Surface Texture from Airborne Laser Scanning Data for the Supervised and Unsupervised Prediction of Area-Based Forest Characteristics." *Remote Sensing* 8 (7): 582. https://doi.org/10.3390/rs8070582.

O'Loughlin, F. E., R. C. Paiva, M. Durand, D. E. Alsdorf, and P. D. Bates. 2016. "A Multi-Sensor Approach Towards a Global Vegetation Corrected SRTM DEM Product." *Remote Sensing of Environment* 182:49–59. https://doi.org/10.1016/j.rse.2016.04.018.

Potapov, P., X. Li, A. Hernandez-Serna, A. Tyukavina, M. C. Hansen, A. Kommareddy, A. Pickens, et al. 2021. "Mapping Global Forest Canopy Height Through Integration of GEDI and Landsat Data." *Remote Sensing of Environment* 253 (February): 112165. https://doi.org/10.1016/j.rse.2020.112165.

Pretzsch, H. 2009. *Forest Dynamics, Growth and Yield: From Measurement to Model*. Berlin, Heidelberg: Springer. https://doi.org/10.1007/978-3-540-88307-4.

Probst, A., D. Gatziolis, and N. Strigul. 2018. "Intercomparison of Photogrammetry Software for Three-Dimensional Vegetation Modelling." *Royal Society Open Science* 5 (7): 172192. https://doi.org/10.1098/rsos.172192.

Repola, J. 2008. "Biomass Equations for Birch in Finland." *Silva Fennica* 42 (4): 605–624. https://doi.org/10.14214/sf.236.

Repola, J. 2009. "Biomass Equations for Scots Pine and Norway Spruce in Finland." *Silva Fennica* 43 (4): 625–647. https://doi.org/10.14214/sf.184.

Rizzoli, P., M. Martone, C. Gonzalez, C. Wecklich, D. Borla Tridon, B. Bräutigam, M. Bachmann, D. Schulze, T. Fritz, and M. Huber. 2017. "Generation and Performance Assessment of the Global TanDEM-X Digital Elevation Model." *ISPRS Journal of Photogrammetry & Remote Sensing* 132:119–139. https://doi.org/10.1016/j.isprsjprs.2017.08.008.

Rodriguez, E., C. S. Morris, and J. E. Belz. 2006. "A Global Assessment of the SRTM Performance." *Photogrammetric Engineering & Remote Sensing* 72 (3): 249–260. https://doi.org/10.14358/PERS.72.3.249.

Rosier, I., J. Diels, B. Somers, and J. Van Orshoven. 2021. "A Workflow to Extract the Geometry and Type of Vegetated Landscape Elements from Airborne LiDAR Point Clouds." *Remote Sensing* 13 (20): 4031. https://doi.org/10.3390/rs13204031.

Roussel, J.-R., D. Auty, N. C. Coops, P. Tompalski, T. R. H. Goodbody, A. S. Meador, J.-F. Bourdon, F. De Boissieu, and A. Achim. 2020. "LidR: An R Package for Analysis of Airborne Laser Scanning (ALS) Data." *Remote Sensing of Environment* 251:112061. https://doi.org/10.1016/j.rse.2020.112061.

Seidl, R., D. Thom, M. Kautz, D. Martin-Benito, M. Peltoniemi, G. Vacchiano, J. Wild, D. Ascoli, M. Petr, and J. Honkaniemi. 2017. "Forest Disturbances Under Climate Change." *Nature Climate Change* 7 (6): 395–402. https://doi.org/10.1038/nclimate3303.

Skidmore, A. K., N. C. Coops, E. Neinavaz, A. Ali, M. E. Schaepman, M. Paganini, W. D. Kissling, P. Vihervaara, R. Darvishzadeh, and H. Feilhauer. 2021. "Priority List of Biodiversity Metrics to Observe from Space." *Nature Ecology & Evolution* 5 (7): 896–906. https://doi.org/10.1038/s41559-021-01451-x.

Stefanidou, A., I. Z. Gitas, L. Korhonen, D. Stavrakoudis, and N. Georgopoulos. 2020. "Lidar-Based Estimates of Canopy Base Height for a Dense Uneven-Aged Structured Forest." *Remote Sensing* 12 (10): 1565. https://doi.org/10.3390/rs12101565.

Stereńczak, K., G. Vaglio Laurin, G. Chirici, D. A. Coomes, M. Dalponte, H. Latifi, and N. Puletti. 2020. "Global Airborne Laser Scanning Data Providers Database (GLOBALS)—A New Tool for Monitoring Ecosystems and Biodiversity." *Remote Sensing* 12 (11): 1877. https://doi.org/10.3390/rs12111877.

Straub, C., J. Tian, R. Seitz, and P. Reinartz. 2013. "Assessment of Cartosat-1 and WorldView-2 Stereo Imagery in Combination with a LiDAR-DTM for Timber Volume Estimation in a Highly Structured Forest in Germany." *Forestry* 86 (4): 463–473. https://doi.org/10.1093/forestry/cpt017.

Toivonen, J., A. Kangas, M. Maltamo, M. Kukkonen, and P. Packalen. 2023. "Assessing Biodiversity Using Forest Structure Indicators Based on Airborne Laser Scanning Data." *Forest Ecology & Management* 546:121376. https://doi.org/10.1016/j.foreco.2023.121376.

Tompalski, P., J. C. White, N. C. Coops, M. A. Wulder, A. Leboeuf, I. Sinclair, C. R. Butson, and M.-O. Lemonde. 2021. "Quantifying the Precision of Forest Stand Height and Canopy Cover Estimates Derived from Air Photo Interpretation." *Forestry: An International Journal of Forest Research* 94 (5): 611–629. https://doi.org/10.1093/forestry/cpab022.

Ullah, S., M. Dees, P. Datta, P. Adler, T. Saeed, M. Sadiq Khan, and B. Koch. 2020. "Comparing the Potential of Stereo Aerial Photographs, Stereo Very High-Resolution Satellite Images, and Tandem-X for Estimating Forest Height." *International Journal of Remote Sensing* 41 (18): 6976–6992. https://doi.org/10.1080/01431161.2020.1752414.

Vastaranta, M., X. Yu, V. Luoma, M. Karjalainen, N. Saarinen, M. A. Wulder, J. C. White, H. J. Persson, M. Hollaus, and T. Yrttimaa. 2018. "Aboveground Forest Biomass Derived Using Multiple Dates of WorldView-2 Stereo-Imagery: Quantifying the Improvement in Estimation Accuracy." *International Journal of Remote Sensing* 39 (23): 8766–8783. https://doi.org/10.1080/01431161.2018.1492176.

Wagner, C. E. V. 1977. "Conditions for the Start and Spread of Crown Fire." *Canadian Journal of Forest Research* 7 (1): 23–34. https://doi.org/10.1139/x77-004.

Wing, B. M., M. W. Ritchie, K. Boston, W. B. Cohen, and M. J. Olsen. 2015. "Individual Snag Detection Using Neighborhood Attribute Filtered Airborne LiDAR Data." *Remote Sensing of Environment* 163:165–179. https://doi.org/10.1016/j.rse.2015.03.013.

Wittke, S., X. Yu, M. Karjalainen, J. Hyyppä, and E. Puttonen. 2019. "Comparison of Two-Dimensional Multitemporal Sentinel-2 Data with Three-Dimensional Remote Sensing Data Sources for Forest Inventory Parameter Estimation Over a Boreal Forest." *International Journal of Applied Earth Observation and Geoinformation* 76:167–178. https://doi.org/10.1016/j.jag.2018.11.009.

Woods, M., K. Lim, and P. Treitz. 2008. "Predicting Forest Stand Variables from Lidar Data in the Great Lakes St. Lawrence Forest of Ontario." *The Forestry Chronicle* 84 (6): 827–839. https://doi.org/10.5558/tfc84827-6.

Yin, T., P. M. Montesano, B. D. Cook, E. Chavanon, C. S. Neigh, D. Shean, D. Peng, N. Lauret, A. Mkaouar, and O. Regaieg. 2023. "Modeling Forest Canopy Surface Retrievals Using Very High-Resolution Spaceborne Stereogrammetry: (II) Optimizing Acquisition Configurations." *Remote Sensing of Environment* 298:113824. https://doi.org/10.1016/j.rse.2023.113824.

Zink, M., A. Moreira, I. Hajnsek, P. Rizzoli, M. Bachmann, R. Kahle, T. Fritz, M. Huber, G. Krieger, and M. Lachaise. 2021. "Tandem-X: 10 Years of Formation Flying Bistatic SAR Interferometry." *IEEE Journal of Selected Topics in Applied Earth Observations & Remote Sensing* 14:3546–3565. https://doi.org/10.1109/JSTARS.2021.3062286.

Zolkos, S. G., S. J. Goetz, and R. Dubayah. 2013. "A Meta-Analysis of Terrestrial Aboveground Biomass Estimation Using LiDAR Remote Sensing." *Remote Sensing of Environment* 128:289–298. https://doi.org/10.1016/j.rse.2012.10.017.

Zvoleff, A. 2020. "GLCM." R Package. Accessed September 2, 2025. https://cran.r-project.org/web/packages/glcm/index.html.